This document is the accepted manuscript version of the following article:

Lavrieux, M., Schubert, C. J., Hofstetter, T., Eglinton, T. I., Hajdas, I., Wacker, L., & Dubois, N. (2017). From medieval land clearing to industrial development: 800 years of human-impact history in the Joux Valley (Swiss Jura). Holocene, 27(10), 1443-1454. https://doi.org/10.1177/0959683617693892

**Research paper**

# From medieval land clearing to industrial development:

# 800 years of human impact history in the Joux Valley (Swiss Jura)

Marlène Lavrieux[1,2], Carsten J Schubert[3], Thomas Hofstetter[1], Timothy I Eglinton[4], Irka Hajdas[5], Lukas Wacker[5] and Nathalie Dubois[1,4]

[1]Eawag, Swiss Federal Institute of Aquatic Science and Technology, Dübendorf, Switzerland

[2]University of Basel, Department of Environmental Science, Basel, Switzerland

[3]Eawag, Swiss Federal Institute of Aquatic Science and Technology, Kastanienbaum, Switzerland

[4]Geological Institute, Department of Earth Sciences, Swiss Federal Institute of Technology Zurich (ETHZ), Zürich, Switzerland

[5]Laboratory of Ion Beam Physics, Swiss Federal Institute of Technology Zurich (ETHZ), Zurich, Switzerland

**Corresponding author**:

Marlène Lavrieux – Current address: Environmental Geosciences, Department Environmental Sciences, University of Basel, Bernoullistrasse 30, 4056 Basel, Switzerland.

Email: marlene.lavrieux@unibas.ch

## Abstract

The Joux Valley (Swiss Jura Mountains) has a rather unusual history of human occupation, characterized by tardive but extensive settlement since the Late Middle Ages, followed by an intensive period of industrial development. To estimate the links between human activities and environmental consequences

in the area, sediment cores were retrieved in Lake Joux and submitted to a multiproxy analysis (high-resolution photographs, magnetic susceptibility, density, X-ray fluorescence, grain size, organic geochemistry, $^{14}C$, $^{210}Pb$ and $^{137}Cs$ dating). The diversity of anthropication phases, defined from historical data, is clearly recognized in the lake archive. The sediment record suggests the region was mainly under natural (climatic) influence until the end of the 13th century. The growth of settlements in the valley and the associated massive deforestation is recorded by increasing terrestrial inputs, reflecting large-scale soil destabilization in the area, which subsequently persists despite the transition from farming to industrial activities. Autochthonous contributions then dominate the record, both in response to climatic and anthropogenic influences. Construction works conducted at the outlet of the lake affected water flow, sedimentation and aquatic community (macrophytes, ostracods) dynamics. The substantial increase of anthropogenic heavy metals (Fe, Zn, Pb) recorded during the 20th century could reflect the development of the watch-making industry in the area, as well as the use of leaded gasoline. Historical information facilitated interpretation of the observed paleolimnological evolution in the context of varied coexisting human activities. This study highlights the importance of applying an integrated paleolimnological-historical approach in order to establish clear links between well-defined human activities and their subsequent environmental responses through time.

**Keywords**

Lake sediments, multiproxy analysis, historical information, land clearing, industry, Swiss Jura

## Introduction

During the Holocene, humans have emerged as a major geologic agent (Hooke, 2000), transforming between one third and one half of the terrestrial surface (Vitousek et al., 1997; Messerli et al., 2000). Large-scale human-driven alterations of the environment are now becoming a serious threat for the

sustainability of ecosystems and human activities, including agriculture and the exploitation of natural resources (Vitousek et al., 1997; Messerli et al., 2000). Indeed, land-use changes and agricultural practices are highlighted as key factors in soil degradation, as they increase erosion and decrease fertility. They also form the main drivers of biodiversity loss in terrestrial and freshwater ecosystems and of the eutrophication of waters (Lal, 1997; Sala et al., 2000; Smith, 2003; Wilkinson, 2005; Dudgeon et al., 2006; Rumpel et al., 2009). Ecological systems are also affected by toxic heavy metals that are released to soil, freshwaters and air through mining, industrial activities and sewage (e.g. Bryan, 1971; Giller et al., 1998). The simultaneous occurrence of several activities which can have the same environmental consequences often makes it difficult to link known anthropogenic disturbances with their corresponding environmental responses. While natural archives bring information about environmental conditions before and after human influences, historical documents afford precise insights into the occurrence and precise timing of human activities on local to regional scales. Studies that integrate natural archives and historical data are much needed in order to validate hypotheses about the interconnections between societies and ecological systems (Dearing, 2006, 2013; Dearing et al., 2006).

Due to its remote location in the Swiss Jura Mountains, extensive settling of the Joux Valley only dates back to the Middle Ages. As one of the birthplaces of Swiss horology, human activities and land use history of this valley have been extensively documented in historical investigations (e.g. Nicole, 1840; Golay, 1891; Piguet, 1946, 1947, 1952, 1971, 1999; Rochat, 1995, 2006), maps (e.g. Anonymous, 1572; Layné, 1671; Vallotton, 1708) and travelogues (e.g. Correvon, 1737). Sedimentary records from the Joux area have already shown potential for palaeoenvironmental and palaeoclimatic studies (e.g. Wegmüller, 1966; Mitchell et al., 2001; Magny et al., 2008). Despite revealing a decoupling between human activities and climatic conditions, these prior studies did not allow in-depth assessment of the processes linking specific past human activities to their environmental consequences. In particular, (1) the links between the development of settlements and soil erosion and (2) potential signatures of past

industrial activity recorded in Lake Joux sediments have never been explored. While for many sites, the lack of historical information or the absence of sedimentary record hampers the exploration of both archives, the wealth of historical information on the Joux Valley renders it a perfect case study to investigate direct links between different types of human activity with their environmental consequences. Here, various proxies (e.g. physical, geochemical) recorded in the core, can be attributed to the respective effects of diverse co-occurring human activities (farming, industries). We apply this integrated approach to a 1150-year-long sedimentary record, where multiproxy analysis (using high-resolution magnetic susceptibility and XRF core scanning, grain-size distribution, (organic) geochemical analyses, radiocarbon, $^{210}$Pb and $^{137}$Cs dating, high-resolution pictures) is reconciled with historical information.

## Site and methods

### *Study site*

The Joux Valley is located in the Jura Mountains (Fig. 1), traversing the Swiss-French border. The valley developed in a Jura syncline, marked by glacial (wurmian) erosion and Quaternary deposits. It lies mainly on Upper Jurassic and Tertiary limestones, and extends over ca. 30 km in a SW-NE orientation (Aubert, 1941a, b) with mean elevation > 1000 m above sea level (a.s.l.). Four lakes lie in its thalweg (Lake Rousses, Lake Joux, Lake Ter and Lake Brenet), which is flanked by 1300-1600 m a.s.l. mountains. The area is characterized by a semi-continental climate, with a mean annual temperature of 6°C and mean annual precipitation of 1500-2000 mm (30% snow; Fuchs, 2008). Lake Joux (1004 m a.s.l.) has an average depth of 32 m and a water surface area of ca. 9 km$^2$ and a watershed area of ca. 211 km$^2$. The lake freezes almost every winter and the ice break-up occurs between March and the beginning of May (Baud, 1970). The lake is mainly fed by the meandering Orbe River, one of the last unmodified rivers in Switzerland, with a mean annual discharge of 2.2 m$^3$/s (Paquet, 2002). Several small streams located on its eastern shore also supply minor amounts of water and sediment to lake, particularly during intense

episodes of precipitation. Lake Brenet and karstic caves are the main outlets of the lake, the latter becoming inlets during heavy rainfall events (Aubert, 1943). The Orbe River re-emerges 3 km downstream of the lake.

The first evidence of human presence in the Lake Joux catchment dates back to as early as 6850 cal. yr BP (forest grazing, first pastures; Mitchell et al., 2001), and a continuous human presence is recorded since the Roman period (Wegmüller, 1966). A monastery existed on the shores of Lake Ter during the 5$^{th}$ – 6$^{th}$ centuries (Fig. 1), followed by the foundation of Lake Joux Abbey in L'Abbaye in 1126 CE, which subsequently disappeared after 450 years of domination over the valley. The valley then became extensively settled in the 14$^{th}$ century during which forests were cleared to breed cattle, and later wood and hydraulic force were used for sawmills and the metal industry (Piguet, 1947). Recurrent bad harvests and food shortages prompted the development of glasswork and lapidary industries in the late 17$^{th}$ century (Nicole, 1840). Horology was introduced to the valley a century later, and became a major economic activity in the 19$^{th}$ century. This industrialization of the valley resulted in the progressive replacement of cultivated fields by grazing areas and fallows. At the end of the 19$^{th}$ century, the natural connection between Lakes Joux and Brenet was filled and replaced by a canal slightly further west when the railway under construction. Virtually simultaneously, in 1901, a hydroelectric power plant was constructed at the eastern end of Lake Brenet and all the karstic cave outlets were sealed (cemented) in an effort to regulate both lake levels. In 1942, a gallery was dug between the two lakes, deeper than the original canal in order to allow sufficient water flow into Lake Brenet even in times of intense drought (Calame and Paschoud, 1946). Nowadays, the valley is mainly covered by forests and high mountain pastures, and is renowned for its luxury horology and as a winter sports resort.

***Coring and lithological correlation***

A 70-cm-long core (JOU-13-02; 46.6399°N, 6.2875°E) and an 85.5-cm-long core (JOU-14-01; 46.6401°N, 6.2866°E) were retrieved in the central distal part of the lake using a gravity corer, at 35 and 34.1 m water depth, respectively. The occurrence of numerous key horizons allowed facile and precise correlation of the two cores (Supplementary Fig. 1, available online). Both cores were sampled to ensure enough sedimentary material for the different subsequent analyses. Unless explicitly specified, the depths cited in this study refer to JOU-14-01, as most of the analyses were performed on this core. All the data used for this study are available online in supplementary Table 1.

***Non-destructive measurements (high-resolution photographs, XRF, magnetic susceptibility)***

High-resolution photographs of the fresh sediment surface were taken immediately after opening the cores. Non-destructive magnetic susceptibility and X-ray fluorescence (XRF) core scanning were performed on the 2 cores using a Geotek Multi-Sensor Core Logger (resolution: 5 mm) and an Avaatech core scanner with a vertical step of 2 mm as described in Wirth et al. (2013), respectively. Here we only considered the following diagnostic elements:(1) Ca for autochthonous contributions, (2) Ti and K for terrestrial inputs, and (3) Pb, Zn and Fe as markers of early human impacts. To examine the statistical correlations between elements and delineate the unit boundaries, a principal component analysis (PCA) was performed on the XRF data using XLStat 18.06 (Addinsoft, Inc., Brooklyn, NY, USA, 2016) (Fig. 3). With K being more concentrated in non-weathered minerals, the K/Ti ratio was used to estimate the chemical weathering (Arnaud et al., 2012). Variations in terrigenous flux were assessed by calculating Ti flux according to Arnaud and Révillon (2015).

***Grain-size distribution***

The grain-size distribution of the sediment was determined at a 1 cm resolution using a Malvern Mastersizer 2000 (Malvern Instruments Ltd) laser particle size analyzer. Samples were dispersed in

$NaPO_4$ prior to analysis and disaggregated by ultrasonication. Each sample was measured at least three times.

***Isotopic and geochemical analyses***

The working half of core JOU-13-02 was sliced for isotopic and geochemical analyses and for radiocarbon dating. The basic sampling resolution was 1 cm, although this was slightly adjusted when needed so that no sample would contain two different lithologies. Samples were freeze-dried and ground and their total carbon (TC) content was measured using an elemental analyzer (EURO EA 3000). Total inorganic carbon (TIC) content was obtained from a titration Coulometer (CM5015) and $CaCO_3$ content was calculated as $CaCO_3$=TIC*8.33. Total organic carbon (TOC) was calculated as TOC = TC – TIC.

After decarbonatation, the stable carbon isotopic composition of bulk organic matter was determined using a continuous flow isotope ratio mass spectrometer (Micromass Isoprime) coupled to a Carlo-Erba elemental analyzer. C isotope ratios are reported as $\delta^{13}C_{org}$. δ values are ‰-deviation from the carbon isotopic composition of the Vienna Pee Dee Belemnite (VPDB) standard: $\delta^{13}C_{org} = [(R_{sample}/R_{standard}) - 1] \times 1000$, where $R$ is the $^{13}C/^{12}C$ ratio. Average standard deviations based on replicate measurements were better than 0.2‰.

Phosphorus concentrations in the core were too low for reliable detection based on the XRF signal, and were instead measured following the method of Reinhard et al. (2005) using a Flow Injection Analyzer (SAN++, SKALAR).

36 samples were chosen along the JOU-14-01 core for inductively coupled plasma mass spectrometry (ICP-MS) measurements. 50 mg of dried and crushed sediment were digested using a mixture of 1.5 ml of nitric acid ($HNO_3$, 65%) and 0.1 ml hydrofluoric acid (HF 38%). The resulting solutions were then heated (240°C, 120 bar, 10 minutes) in an ultraclave system (Milestone srl, Sorisole,

Italy) and subsequently transferred into polyethylene flasks, the levels of which were adjusted to 10 ml with nanopure water. Samples were diluted 1/50 and analyzed by ICP-MS (Agilent Technologies 7500 Series, Santa Clara, CA, USA), with metal concentrations determined using a calibration curve from a multi-elemental internal standard. The reproducibility of the measurements, based on replicate standard analysis, is better than 10 %.

***Molecular organic geochemical (biomarker) analyses***

19 sediment samples were taken along JOU-14-01 core for biomarker analysis. 2-5 g of freeze-dried and homogenized sediments were microwave-extracted using $CH_2Cl_2$:MeOH (4:1). After removal of the solvent under $N_2$, hydrocarbon fraction (containing *n*-alkanes) was isolated from the lipid mixture by elution with hexane (4 mL) through an aminopropyl-bonded silica column. Purified samples were injected on an Agilent 7890B Gas Chromatograph with Flame Ionization Detector (GC-FID). The instrument was fitted with an Agilent 19091J-413 column (30 m * 0.32 mm i.d., 0.25 µm film thickness). The operating conditions were: 50°C (1 min) to 320°C at 10°C.min$^{-1}$, hold 5 min, then to 100°C at 100°C.min$^{-1}$. Samples were injected in splitless mode, with the injector at 250°C. $H_2$ was the carrier gas. Compounds were identified and quantified by comparison of retention times and elution patterns with a mixture of *n*-alkane standards. Concentrations, which were well above detection limits, were estimated by measuring peak areas on chromatograms.

Long-chain (i.e. > 20 carbons) *n*-alkane distribution patterns are widely used in the form of ratios as indicators of vegetation inputs and climatic variations in sediments:

1. Vegetation type can be assessed from the ratio ($C_{27}$+$C_{29}$/$C_{31}$), as grasses are characterized by a high relative abundance of $C_{31}$, while the dominant homologue in trees is either $C_{27}$ or $C_{29}$ (Cranwell, 1973; van Bergen et al., 1997).

2. The Carbon Preference Index (CPI), representing the relative proportion of even versus odd *n*-alkanes, depends on the extent of land vegetation input (Bray and Evans, 1961) and on microbial degradation, with the latter assumed to be more intense in warmer climates (Zhang et al., 2014, and references therein). In specific contexts, it can also be influenced by anthropogenic hydrocarbon and sedimentary rocks inputs. It is calculated as

$$0.5 \times \left(\frac{C_{25} + C_{27} + C_{29} + C_{31} + C_{33}}{C_{24} + C_{26} + C_{28} + C_{30} + C_{32}} + \frac{C_{25} + C_{27} + C_{29} + C_{31} + C_{33}}{C_{26} + C_{28} + C_{30} + C_{32} + C_{34}}\right)$$

3. The Average Chain Length (ACL) describes the weighted mean *n*-alkane chain length and varies with vegetation type (van Bergen et al., 1997), as well with environmental factors such as climate: the rationale is that in warmer conditions, plants synthesize longer chain wax lipids than in cooler climates to avoid water losses through evaporation (Gagosian and Peltzer, 1986). It is defined as

$$\frac{\sum(C_i \times [C_i])}{\sum[C_i]}$$

where $[C_i]$ is the concentration of the *n*-alkane of carbon number $C_i$, over the range 23-33 (after Poynter and Eglinton, 1990).

4. Paq provides an indication of relative contributions from aquatic macrophytes (producing more $C_{23}$ and $C_{25}$) vs. vegetal terrestrial plants (producing more $C_{29}$ and $C_{31}$) to lake sediments (Ficken et al., 2000)

$$\frac{C_{23} + C_{25}}{C_{23} + C_{25} + C_{29} + C_{31}}$$

***Dating***

The Joux limestone catchment delivers old carbon to the lake that can affect the sediment $^{14}C$ chronology. To avoid this hard-water effect, $^{14}C$ was measured on terrestrial macrofossils. Fresh JOU-13-02 samples were sieved (500 µm) under MilliQ water. A stereomicroscope was used to hand-pick the terrestrial macrofossils (mainly wood, insect parts, leaves and vegetal debris) in the > 500 µm fraction. The largest samples (13) were selected and washed with the standard procedure of acid-base-acid treatment (ABA, 30 min, 60°C; e.g. Hajdas et al., 2014). Samples that contained more than 200 µg of carbon were graphitized using AGE system (Wacker et al., 2010) and all that were smaller were flame-sealed under vacuum in quartz tubes containing pre-combusted CuO, and oxidized to $CO_2$ overnight at 950°C. $CO_2$ was then transferred to a calibrated volume where pressure was sensor-measured by cracking the tubes under vacuum. A dry ice/ethanol mixture was used to separate water from $CO_2$. The latter was transferred to Pyrex tubes and flame sealed under vacuum for AMS measurement, which were performed on the miniaturized radiocarbon dating system (MICADAS; Synal et al., 2007) at the laboratory of Ion Beam Physics of the ETH Zürich.

The chronology of the upper part of core JOU-13-02 is based on $^{137}Cs$ and $^{210}Pb$ measurements. 5-10 g of 16 freeze-dried and ground sediment samples were weighted into sample tubes. The samples were measured using a high-purity Germanium (HPGe) Well Detector (Gamma spectrometer).

## Results

### *Depth-age model*

The occurrence of rapidly deposited layers (RDL; e.g. floods events, mass wasting deposits) in the core was carefully assessed prior to building the depth-age model. As instantaneous deposits, these layers must to be removed to avoid the distortion of the actual background sedimentation rate. No erosive layer was detected in the whole archive, and the visual observation indicates uninterrupted sedimentation over the

entire length of the core. Moreover, though Ti shows local maximums throughout the core, its evolution does not exhibit the sharply contrasted pattern that usually discriminates flood deposits from background sedimentation (e.g. Lavrieux et al., 2013). From the available data, the major floods having affected the Joux Valley described in literature (1571, 1600, 1751, 1817, 1863, 1867, 1883, 1888, 1899, 1910; Golay-Nicole, 1994) are not visible in the sediment record. Therefore, based on sedimentological evidence, no RDL was identified in the Joux cores.

The $^{137}$Cs profile exhibits a single peak instead of the 2 usually measured in Swiss Lake sediments (corresponding to the 1986 Chernobyl accident and the 1963 maximum fallout resulting from atmospheric nuclear bomb tests; Fig. 2). A "non-recording" of the 1986 peak can be excluded as the Joux Valley was recognized as one of the regions of Switzerland most affected by Chernobyl fallout (Swiss Federal Nuclear Safety Inspectorate, 2016). The single broad peak (13-7 cm depth) thus most probably indicates mixing through bioturbation of the uppermost sediments, which nevertheless remains slight given the continuous trend of $^{210}$Pb. The sedimentation rate calculated from the latter is 0.22 cm/yr, giving an indicative age of 1936 CE at 18 cm depth. This is slightly older than the first detection of $^{137}$Cs activity, i.e. ca. 1954 CE (sedimentological first record of this artificial radionuclide in Switzerland; e.g. Thevenon and Poté, 2012), observed at 16 cm depth.

A total of 13 macrofossil samples (each sample including several specimen isolated from the same sediment layer) from JOU-13-02 were radiocarbon dated (Table 1). One age from the very recent part (8-9 cm depth) was calibrated with CaliBomb (http://calib.qub.ac.uk/CALIBomb/, accessed 2015) using IntCal13 and Levin bomb curve extension. Its calibrated age is consistent with $^{210}$Pb age calculated for the same horizon (1981 CE ± 4 yrs 2σ and 1976 CE, respectively). The other ages were calibrated using the Bayesian deposition model of OxCal to reduce uncertainties on calendar ages (e.g. Blaauw et al., 2007; Hajdas, 2014) with OxCal 4.2.4, using the IntCal13 data set (http://c14.arch.ox.ac.uk/oxcal,

accessed 2016). Two ages were excluded because they gave aberrant ages that were incompatible with the sedimentological observations. Ages were calculated for each depth (Supplementary Table 1). According to the output model, the 68cm-long sequence of JOU-13-02 covers the last 1000 years. The extrapolation of the model suggests an age of ca. 1150 years (i.e. ca. 860 CE) for the base of the JOU-14-01 sequence. The sedimentation rate varies along the JOU-13-02 core (Fig. 5): between 0.04-0.08 cm/yr from the base (U1) to the beginning of U4, with a notable maximum up to 0.11 cm/yr during the first half of the 15$^{th}$ century (U2a), then 0.03 cm/yr during U4, 0.83 cm/yr at the transition from U4 to U5, decreasing to 0.18 cm/yr for the last 60 years.

***Sedimentological features and core description***

The XRF Ca signal being redundant with the $CaCO_3$, only the latter is considered hereafter. XRF results were calibrated using ICP-MS data (Fig. 4, Supplementary Fig. 2). A significant positive correlation was observed between the XRF and ICP-MS signals for Ti, K, Pb, Zn and Fe ($R^2$= 0.78, 0.63, 0.71, 0.86, 0.70, respectively; Fig. 4). Correlation is higher when excluding the lowest 14 cm of the core ($R^2$=0.86, 0.76, 0.77, 0.88, 0.74, respectively). This lower correlation can be explained by the larger grain-size of this lower section of the core (Fig. 5).

Ti, Al, Fe and K are widely used to characterize detrital sediments and their dynamics (e.g. Revel-Rolland et al., 2005; Arnaud et al., 2012; Lavrieux et al., 2013), but metal elements such as Fe and Al must be used cautiously in catchments like the Joux Valley were industrial activity may also serve as a source for these elements. Ti, which is highly correlated to K ($R^2$=0.945), was chosen as the most reliable element for tracing detrital inputs in this study, as it showed the best correlation between XRF and ICP-MS data (Fig. 4). To distinguish detrital from industrial inputs, heavy metals were normalised to Ti (Fig. 5). The PCA analysis highlights correlations between elements, distributed in 3 pools in the Dimension 1 vs. Dimension 2 plot (Fig. 3): (1) Fe, Ti and K, (2) Zn and Pb, and (3) Ca. Dimensions 1 and 2 represent

86.64% of the variability. Visual observation, sedimentological, organic and inorganic features, and the composite signature integrated in the magnetic susceptibility signal allow the distinction of 5 sedimentary units (Fig. 5).

1. Unit 1 (U1, 85-63 cm) shows alternating dark brown and slightly lighter layers with 4-7% of OM. The PCA analysis shows a positive correlation of this unit with Ti, K and Fe (Fig. 3). Magnetic susceptibility is relatively stable, with the exception of a decrease and a subsequent increase at the top of the unit. Ti generally shows local maxima in the darker layers. The only dark layer analysed for grain size shows it to be coarser grained with a much higher sand content than the surrounding samples. While selecting macrofossils for radiocarbon dating, stereomicroscope observations showed a qualitatively and quantitatively similar macrofossil content in the two types of layer, consisting mainly of terrestrial debris mixed with chironomid pupae and cephalic capsules, ostracods valves, and a few bivalves, the latter being better preserved in the brown layers. Both types of layers exhibit similar organic carbon content and $\delta^{13}C$ values. Grain size decreases towards the top of the unit, while K/Ti increases. In one of the light layer samples, significantly higher Paq the value indicates a higher algal contribution (Meyers and Lallier-Vergès, 1999; Ficken et al., 2000), while the relatively high $(C_{27}+C_{29})/C_{31}$ value indicates a more forested catchment.

2. Unit 2 (U2, 63-45 cm) consists of less contrasting alternating layers showing (1) slightly lower organic content than in U1 (4-5% $C_{org}$), (2) lower values of Paq and $(C_{27}+C_{29})/C_{31}$, (3) minor changes in CPI and ACL compared to Unit 1 and (4) slightly higher $\delta^{13}C_{org}$ values, especially towards the top of the unit. Following a ca. 10% increase of the silt fraction evident in the lowest third of the unit, the grain size distribution remains quite stable. The unit also exhibits a positively correlation with Ti, K and Fe, while K/Ti values decrease along the unit. Based on

magnetic susceptibility, sedimentation rate and Ti flux records, this unit is further subdivided into:

- Unit 2a (U2a, 63-55 cm) showing magnetic susceptibility and XRF characteristics comparable to Unit 1, the base of which is marked by a local maximum in magnetic susceptibility and a local minimum in Ti;
- Unit 2b (U2b, 55-45 cm) where sedimentation rate, Ti flux and magnetic susceptibility values significantly increase, the latter reaching its maximum.

3. Unit 3 (U3, 45-27 cm) is also comprised of faintly laminated sediments but is lower in organic carbon (3-4%). It contains many algal remains (esp. 43-34 cm) and shows a decreasing trend in magnetic susceptibility and Ti, both anti-correlated with $CaCO_3$. Accordingly, this unit is correlated with Ti, K and Fe and Ca pools in the PCA analysis. K/Ti is stable throughout the unit while $\delta^{13}C_{org}$ increases in the first third of the unit and then gradually decreases and CPI and ACL trend towards lower values at shallower depth intervals.

4. Unit 4 (U4, 27-15 cm) is characterized by significantly lower organic contents (2-3%) and lower magnetic susceptibility values with the latter markedly increasing at the very end of the unit. It consists of (1) a disturbed bioturbated layer which transitions to a lighter-coloured calcium carbonate rich interval that is depleted in $C_{org}$ (27-24 cm), (2) a light calcium carbonate layer enriched in algal remains (25-17 cm), and (3) a progressive transition to a darker sediment (17-15 cm). The Ti flux gradually decreases along the unit but shows a strong increase at its very end, while Pb/Ti, and Fe/Ti ratios for the first time exceed the background values previously measured. These observations are confirmed by PCA analysis, which reveals a strong correlation of the whole unit with Ca, as well as with Zn and Pb towards the end of the unit. K/Ti values are on average stable,

though more variable than in previous units. The sedimentation rate for this interval is very low (0.03 cm/yr). All the *n*-alkanes based proxies exhibit contrasting values, with CPI and ACL significantly increasing towards the top of the unit. $\delta^{13}C_{org}$ shows a local maximum.

5. Unit 5 (U5, 15-0 cm) corresponds to a bioturbated and more organic-rich sediment interval (up to 6% Corg) with a sandy layer at its base. Paq and $(C_{27}+C_{29})/C_{31}$ values are significantly higher than before just above this silty layer. Throughout the unit, and after a maximum, Ti flux and magnetic susceptibility values progressively decline, the latter despite a significant rise of heavy metals (Pb, Zn, Fe). P also shows a noticeable trend towards increasing values while $\delta^{13}C_{org}$ declines.

## Discussion

When combined with historical data, the information provided by sedimentological and (organic) geochemical analyses (Fig. 5) enables discrimination of natural versus anthropogenic contributions to the sedimentary record. The interpreted overall human imprint, as well as the inputs (autochthonous and detrital) and erosion (physical and chemical) patterns, are summarized in Figure 6.

### *U1 – ca. 860-1280 CE*

The oldest sediments retrieved during this study were deposited in the lake when there was already a human presence in the catchment: though still largely forested, the landscape already included meadows, cereal and hemp fields from ca. 320 CE (based on pollen, plant macrofossil and testate amoebae records Wegmüller, 1966, Mitchell et al., 2001). While no real natural baseline state can thus be defined from this core, the anthropogenic impact on sedimentation of Lake Joux can be assumed to be low given the limited forest clearance at that time (Mitchell et al., 2001),. The progressive increase in human shaping of the environment, in particular during the development of the abbey that was founded on the shores of Lake

Joux during the first part of the 12th century, cannot be identified in the sediments, at least from available magnetic susceptibility and XRF data. $\delta^{13}C_{org}$ values are indicative of high autochthonous contribution to sedimentary organic matter (Meyers and Lallier-Vergès, 1999).

Lithological changes observed before the middle of the 14th century in littoral cores were attributed by Magny et al. (2008) to solar- and NAO-driven lake-level variations. Indeed, the Lake Joux water table was highly responsive to climatic conditions prior to construction work was undertaken in the 20th century in order to control lake level fluctuations (Magny et al., 2011). Accordingly, and in the absence of any indices of human imprint in the available data, we interpret the succession of darker/lighter layers observed in (and unique to) U1 as reflecting lake level variations. This unit formed in the distal basin during the lowest lake level phase of the last millennium, as described by Magny et al. (2008), and was characterized by the emersion (estimated as 100-yrs-long) of the littoral platform. Magny et al. (2011) link this lowest lake level phase to a period of maximal values of the $NAO_{ms}$ index (Trouet et al., 2009). During this period, the dark layers observed in JOU-14-01 and JOU-13-02 tend to occur during $NAO_{ms}$ index local minima. Ti content is higher in the dark layers, implying enhanced detrital inputs during these intervals. K/Ti markedly increases from ca. 1080 CE, which can be interpreted as a weakening of the pedogenic processes in the catchment and an increase of the physical erosion (Arnaud et al., 2012). Detrital intensity decreases at the end of the unit, as shown by the drop of Ti content and fluxes and the increase of the proportion of silty and clayey particles.

***U2 – 1280-1525 CE***

The transition from U1 to U2a (1280-1415 CE) is marked by strong variations in Ti content and biomarker parameters. The lower values of Paq, as well as the slight increase of Ti flux throughout U2a suggest increased terrestrial input to the lake, with decreased contribution from trees-covered areas (lower $C_{27}+C_{29})/C_{31}$). We interpret these changes, as well as the associated drop in K/Ti ratios, as reflecting an

increase of the erosion of well-developed soil horizons linked to forest decline. This increased slope destabilization in the catchment could result from wetter climatic conditions and/or more intense human perturbation of the landscape. Literature data supports both hypotheses: Historical records show that the valley was being intensively settled at that time, with extensive deforestation and drainage efforts to create pastures (Piguet, 1947). Magny et al. (2008) describe wetter conditions in the area and a saw-tooth increase of the lake level from 1270 CE, followed by a further intensification of hydrological conditions ca. 1420 CE, coeval to the doubling of the sedimentation rate observed at the transition to U2b (Fig. 5). While this period is recorded by a series of highly contrasting lithologies in the littoral core studied by Magny and colleagues, only faintly contrasting alternating layers are observed in U2. This can be explained by the higher sensitivity of the littoral platform to facies changes relative to distal areas.

The beginning of U2b (1415-1525 CE) coincides with intensive clearing of land in the catchment. At that time, Ti flux rapidly increases, testifying to high detrital inputs, while low K/Ti values indicate greater input of weathered material, probably originating from well-developed soils exposed by clearing. Along the unit, magnetic susceptibility sharply increases, reaching its highest value for the whole core at the transition between U2b and U3. This dramatic increase in magnetic susceptibility cannot be explained solely by increased detrital inputs, implying the occurrence of additional processes such as erosion of metal oxides present in newly exposed topsoils (e.g. Dearing, 1999; Snowball et al., 2000). In the second part of U2b, $\delta^{13}C_{org}$ values start to rise towards its highest values while Paq remain low, indicating a predominantly terrestrial origin of organic matter. All these lines of evidence as consistent with the expansion of human settlements. During this period, deforestation continued (Mitchell et al., 2001; Magny et al., 2008), reaching its maximum around 1500 CE when all the clearable areas had been opened up (Piguet, 1946). The cleared areas were cultivated and grazed (Magny et al., 2008), while the wood was used for the nascent glass-making industry (Piguet, 1946). While deforestation-induced vegetation change does not manifest itself in any substantial shift in CPI or ACL, both exhibit a minor peak around 1500

CE, and the latter then declines throughout U3. This decoupled evolution between clearing-induced vegetation change and n-alkane CPI and ACL suggests that the latter may be sensitive to climate influence, with cooler conditions result in (1) decreased microbial degradation (higher CPI) and (2) synthesis of shorter chain-length plant waxes (lower ACL). The shift observed in the core marks the beginning of the Little Ice Age (LIA), which is also characterized in European mid-latitudes by a wetter climate (Magny et al., 2008).

***U3 – ca. 1525-1790 CE***

At the base of the unit, high $\delta^{13}C_{org}$ values and Ti flux still indicate enhanced terrestrial inputs (Figure 5), attesting to on-going slope destabilization and erosion at least at the multidecadal scale after the end of massive clearing. Throughout the unit, K/Ti ratios are slightly higher than in the prior unit, which could be indicative of an advanced erosional stage of the soils exposed by clearing during the previous century. The gradual decrease in organic content within U3 is accompanied by a decrease in Ti content and flux, and this trend is coeval with an increase in $CaCO_3$ content and a rapid decline of $\delta^{13}C_{org}$ values that would indicate greater lacustrine contributions to the sedimentary record. The declining Ti content and the strong increase in $CaCO_3$ explain the large decrease of magnetic susceptibility observed throughout U3. All these characteristics reflect a stronger autochthonous contribution, confirmed visually by observation of large quantities of algal remains in the lower part of U3. This increased algal contribution to the sediment can result from (1) increased supply of nutrients, introduced during the previous phases of catchment destabilization, driving the algal development, and/or (2) a decrease in the anthropogenic pressure on the soils, lowering detrital inputs, and resulting in less dilution of the autochthonous signal. The latter explanation is consistent with a reduction in human influence between 1530-1700 CE deduced from previous palynological investigations of the sediment record (Magny et al., 2008). This decline in human influence can also be inferred from historical records that indicate an economic reorganization of

the valley during the 16th century. At this time iron mines were opened in the vicinity of Lake Joux and metal processing took place (Piguet, 1895; Rochat, 2006). Interestingly, these is no significant change in heavy metal concentrations in this sediment deposited during this time, in spite of the proximity of mines to Lake Joux (Fig. 1; Piguet, 1895; Rochat, 2006), which may reflect the limited extent of this activity. Though no further clearing of forests took place they were still exploited to supply the glass and blast furnaces. This industrial development caused a first decline in agriculture (-20% of cultivated areas between 1730-1785; Piguet, 1971), with a corresponding reduction in anthropogenic pressure on soils. CPI continues the trend that began in the previous unit, attesting to a continuation of LIA-related colder conditions. Historical documents testify to a harsher climate in the valley at that time, with 34 years with poor harvests and food shortage described during the 18th century stemming from severe frosts and bad weather (Piguet, 1971).

***U4 – ca. 1790 CE – middle of the 20th century***

The lighter sediment characterizing U4 differs sharply from the previous units. Visual observation as well as higher $\delta^{13}C_{org}$ values and $CaCO_3$ contents reveals a strong algal contribution, while (excluding the first data point of the unit) Paq values remain comparable to those of U3. Lower Ti fluxes indicate diminished detrital inputs, while K/Ti values are more variable but on average slightly higher than in U3. Several factors could have led to the increased algal contribution and associated change in sedimentation pattern:

1. *Low lake level*. This unit occurs during a phase of overall low lake water level (Magny et al., 2008), though rapid variations occurred (Nicole, 1840). Interestingly, in 1777, a dike constructed between the Joux and Brenet lakes to tentatively lower the level of the latter suddenly failed shortly after its completion. The water level of Lake Joux dropped by 12 feet (~ 3.6 m) in 24 hours, sweeping away large quantities of sediment and forming a gully in the strait between the two lakes, broadening their connection (Nicole, 1840).

2. *Warmer climatic conditions.* The marked decrease of CPI values and the associated increased ACL values from the middle of the 19$^{th}$ century may reflect enhanced microbial degradation and synthesis of longer chain plant wax lipids, respectively, both consistent with warmer conditions. These trends signal the end of the LIA, lending support to the timing proposed for the area by Magny et al. (2008).
3. *Induced carbonate precipitation.* Lake Joux water is enriched in calcium carbonate (Fuchs, 2008), the solubility of which decreases as temperature increases. Warmer climatic conditions led to the heating of the shallower water body (low lake water level), hence favouring the precipitation of $CaCO_3$. This interpretation is supported by the higher inorganic carbon contents of this unit (higher $CaCO_3$ but lower $C_{org}$) and by the autochthonous character of the carbonate identified for this unit by Bruder (2003).

In tandem with these changes, as a consequence of repeated food shortages, residents of the valley abandoned self-sufficiency and developed a more lucrative watch-making industry during the middle of the 18$^{th}$ century (Piguet, 1895). Consequently, agriculture progressively diminished, with abandoned fields lying fallow. Hence, formerly cultivated soils became less vulnerable to erosion, reducing detrital inputs into the lake. A marked increase of the heavy metals signal (Pb, Zn, Fe) at the very end of this unit testifies to non-detrital heavy metal inputs, which can be directly attributed to industrial activity.

***U5 – Middle of the 20th century – present***

The beginning of the uppermost unit coincides with the occurrence of a second phase of major infrastructure work. The sandy layer observed at the base of U5, which displays the lowest clay content of the whole core and is coincident with a maximum Ti flux, is likely a remnant of building waste that was discharged into the water during the 1942 construction of a subaquatic tunnel to replace the open canal

between the two lakes. This lower gallery was needed to allow sufficient water to flow from Lake Joux into Lake Brenet even during drought years in order to feed the hydroelectric power plant.

Following this event, decreasing $\delta^{13}C_{org}$ values and somewhat higher Paq values indicate an enhanced autochthonous contribution to the sediment. Widespread use of washing machines and washing powders (Bosset, 1981) could explain the higher P inputs into the lake that promotes its eutrophication, as supported by observations based on ostracods assemblages (Whittle, 2006). This eutrophication, together with the abrupt change in grain size coeval to the building of the tunnel, may have triggered the transition from U4 to U5. The aftereffects of the construction on the northern part of the lake was described by Whittle (2006), who observed that it restricted water flow to specific zones, locally affecting sediment dynamics as well as the autochthonous communities (macrophytes, ostracods). However, our results indicate that the impacts on the lake were more widespread and not limited to areas in the vicinity of the tunnel.

Another noteworthy characteristic of Unit 5 is the substantial increase of non-detrital heavy metals (Pb, Zn, Fe), coeval to a drastic drop in Ti flux. An anthropogenic origin for these metals is corroborated by their sharp increase relative to Ti. Prior studies have shown atmospheric inputs of anthropogenically-derived Pb into Swiss natural archives (e.g. lake sediment cores) from the beginning of the 20$^{th}$ century, resulting first from the development of smelting activities, and then from the use of leaded gasoline (introduced into Switzerland in 1947; Shotyk et al., 1996, 2002; Thevenon et al., 2011). As for other industrial activities, the nascent watch-making industry in the Joux Valley would serve as a source of heavy metals to the lake sediments. Insufficient evidence is available to precisely estimate metal contributions from the different types of industry. While the latter is undoubtedly responsible for the heavy metal signature in the sediment archive, the sharp increase in metal concentration at the beginning of U5 does not necessarily mark the intensification of these activities. It could also result from changing

lake dynamics linked to the tunnel construction that modify the signal recorded in underlying sediments. Agricultural spreading of heavy-metal-enriched sludge coming from wastewater treatment plants, a practice established in the Valley since the 1960's (Fiaux et al., 2006), serves as another possible explanation.

Overall, the major changes observed in U5 undoubtedly result from a combination of several events taking place during the 20$^{th}$ century, including tunnel construction, development of the watch industry, eutrophication of the lake and likely also the establishment of wastewater treatment plants.

***Synthesis***

Lake Joux sediments record the evolution of human influence on the lake ecosystem and on the surrounding landscape set against a backdrop of climate variability (Figure 6).

1. The presence of settlers in the catchment prior to the beginning of this record hinders the definition of a pre-anthropogenic baseline conditions for the environment. Marked lithological changes indicate climate-driven water table fluctuations during a period of generally low lake level. Detrital inputs consist of erosion products from well-developed soil horizons. Human impact is not discernible from the available data (U1).
2. With an increase in overall lake level, the climatic imprint on the sedimentary record declined in favor of that derived from intensification of anthropogenic modifications to the landscape (deforestation and drainage). Variations in lake level are no longer discernable in terms of contrasting lithologies, likely due to the combined effects of overprinting of the climatic signal by intensified human activity, and a lower sensitivity of the depositional environment as a consequence of rising lake level. Increased terrestrial inputs and higher terrigenous fluxes attest to the destabilization of the newly exposed soils (U2). Anthropogenic impact on the detrital inputs is clearly evident in the record.

3. As land-clearing reaches its maximum, the development of strong algal signatures is attributed to the influence of prior phases of detrital (nutrient) inputs on the lake ecosystem. Autochthonous inputs from lake productivity continued even when farming pressure on soils were reduced with the emergence of industrial activities (U3).
4. Construction work conducted at the outlet of Lake Joux strongly influenced the lake dynamics (U4-U5): First, at the end of the 18$^{th}$ century, when a dike failure triggered a ~ 3.5 m drop in lake level which, together with economic and climatic factors, resulted in enhanced inorganic carbonate precipitation. Second, in the middle of the 20$^{th}$ century, construction of a subaquatic tunnel led to the development of standing water areas and restricted water flow to specific zones (i.e., northeastern shoreline), promoting eutrophic conditions in the lake (U5). Both eutrophication and changes in lake dynamics changes stemming from tunnel construction are considered to be responsible for the drastic lithological changes observed between U4 and U5.
5. While industrial (including metal) activities were only faintly recorded in the sediments during their early development in the valley, anthropogenic heavy metals are clearly recorded from the middle of the 20$^{th}$ century onwards. Atmospheric deposition, as well as nearby industries (including the local watch-making industry), constitute possible sources of these heavy metals, which are known pollutants for ecosystems (e.g. Wilcock, 1999; Hope, 2006). Potential changes to depositional conditions (and hence the manner in which heavy metal signals are recorded in the sediments) associated with the tunnel construction cannot be excluded, raising broader questions about the environmental consequences of such construction work.

## Conclusion

Though relatively recent, anthropication of the Joux Valley has impacted the local environment in several ways, ranging from extensive farming and massive deforestation, to industrial development and associated construction work. These diverse activities are clearly recorded in the Lake Joux sedimentary archive, enabling appraisal of the reactions of this unique environment to different forms of perturbation. By coupling paleolimnological information with historical data well-defined links between human activities as well as climate variations and their corresponding environmental responses can be established. This coupled approach holds great promise for other locations where both natural and historical archives are available, affording improved characterization of the reactions and the resilience of soils and ecosystems to human-induced disturbances.

**Acknowledgements**

The authors wish to thank S. Bollhalder-Lück, I. Brunner, A. Lück, P. Kathriner, L. Freydier, L. Meuriot, M.B. Roldan Torres de Roettig and M. Maurer for their work in the laboratory, A. Zwyssig, M. Schurter and M. Stockhecke for their help during the coring campaigns, and N. Haghipour and D. Montluçon for their assistance for the biomarkers analysis. We thank Prof. F. Oldfield, Associate Editor. We also appreciate the comments and suggestions of two anonymous reviewers, which greatly improved our manuscript. This work was made possible thanks to an Eawag Discretionary Fund.

**References**

Anonymous (1572) *Pour l'Abbaye Lac de Joux, Baillages de Romainmostier et Morges*. Map, Archives Cantonales Vaudoises.

Arnaud F, Révillon S, Debret M, Revel M, Chapron E, Jacob J, Giguet-Covex C., Poulenard J, Magny M (2012) Lake Bourget regional erosion patterns reconstruction reveals Holocene NW European Alps soil evolution and paleohydrology. *Quaternary Science Reviews* 51: 81-92.

Arnaud F, Révillon S (2015) A geochemical approach to improve radiocarbon-based age-depth models in non-laminated sediment series. In: Croudace IW, Rothwell RG (eds.), *Micro-XRF Studies of Sediment Cores, Developments in Paleoenvironmental Research 17*. Dordrecht: Springer, pp. 459-472.

Aubert D (1941a) *Feuille Vallée de Joux (17). Atlas géologique de la Suisse 1:25000.*Bern (Switzerland): Commission géologique suisse.

Aubert D (1941b) *Notice explicative de la Feuille Vallée de Joux (17). Atlas géologique de la suisse 1:25000.* Bern (Switzerland): Commission géologique suisse.

Aubert D (1943) *Monographie géologique de la Vallée de Joux (Jura Vaudois). Matériaux pour la carte géologique de la Suisse*. Bern (Switzerland): Commission géologique suisse.

Baud P (1970) Débâcles du Lac de Joux. *Feuilles d'Avis de la Vallée de Joux*, 13 May.

van Bergen PF, Bull ID, Poulton PR, Evershed RP (1997) Organic geochemical studies of soils from the Rothamsted classical experiments I - Total lipid extracts, solvent insoluble residues and humic acids from Broadbalk wilderness. *Organic Geochemistry* 26: 117-135.

Blaauw M, Bakker R, Christen JA, Hall VA, van der Plicht J (2007) A Bayesian framework for age-modelling of radiocarbon-dated peat deposits: case studies from the Netherlands. *Radiocarbon* 49, 357-367.

Bosset E (1981) Evolution de l'état sanitaire du Lac de Joux de 1953/57 à 1978/79. *Bulletin de l'Association Romande pour la Protection des Eaux et de l'Air* 108:11-44 and 109:41-64.

Bray EE, Evans ED (1961) Distribution of *n*-paraffins as a clue to recognition of source beds. *Geochimica et Cosmochimica Acta* 22: 2-15.

Bruder PM (2003) *Etudes des sédiments tardi et postglaciaires de la Vallée de Joux (Vaud, Suisse)*. Engineering degree Thesis, University of Geneva, Switzerland.

Bryan (1971) The effects of heavy metals (other than mercury) on marine and estuarine organisms. *Proceedings of the Royal Society of London B* 177: 389-410.

Calame J, Paschoud C (1946) Une amélioration du pouvoir d'accumulation des lacs de Joux et Brenet. *Bulletin technique de la Suisse romande* 72, 1-6.

Correvon GS (1737) Voiage fait à la fin de Juillet 1736 dans les montagnes occidentales du Païs de Vaud. *Mercure Suisse*, July.

Cranwell PA (1973) Chain-length distribution of *n*-alkanes from lake sediments in relation to post-glacial environmental change. *Freshwater Biology* 3: 259-265.

Dearing JA (1999) Holocene environmental change from magnetic proxies in lake sediments. in: Maher BA, Thompson R (eds), *Quaternary Climates, Environments and Magnetism*. Cambridge: Cambridge University Press, pp. 231-278.

Dearing JA (2006) Climate-human-environment interactions: resolving our past. *Climate of the Past* 2: 187-203.

Dearing JA (2013) Why Future Earth needs lake sediment studies. *Journal of Paleolimnology* 49: 537-545.

Dearing JA, Battarbee RW, Dikau R, Larocque I, Oldfield F (2006) Human–environment interactions: towards synthesis and simulation. *Regional Environmental Change* 6: 115–123.

Dudgeon D, Arthington AH, Gessner MO, Kawabata ZI, Knowler DJ, Lévêque C, Naiman RJ, Prieur-Richard AH, Soto D, Stiassny MLJ, Sullivan CA (2006) Freshwater biodiversity: importance, threats, status and conservation challenges. *Biological Reviews* 81: 163-182.

Fiaux JJ, Knispel S, Lods-Crozet B, Strawczynski A, Vioget P, Buttiker B, Gmür P (2006) *Le Lac de Joux et l'Orbe milieux vivants - Evolution de la qualité des eaux : 1985 - 2004*. Lausanne (Switzerland) : Service des eaux, sols et assainissement du canton de Vaud.

Ficken KJ, Li B, Swain DL, Eglinton G (2000) An *n*-alkane proxy for the sedimentary input of submerged/floating freshwater aquatic macrophytes. *Organic Geochemistry* 31: 745-749.

Fuchs M (2008) *Integration of ground-penetrating radar, high-resolution seismic and stratigraphic methods in limnogeology: holocene examples from western Swiss lake deposits*. PhD Thesis, University of Geneva, Switzerland.

Gagosian RB, Peltzer ET (1986) The importance of atmospheric input of terrestrial organic material to deep sea sediments. *Organic Geochemistry* 10: 661–669.

Giller KE, Witter E, Mcgrath SP (1998) Toxicity of heavy metals to microorganisms and microbial processes in agricultural soils: a review. *Soil Biology and Biochemistry* 30: 1389-1414.

Golay H (1891) *La Vallée de Joux, 1860 à 1890*. Lausanne (Switzerland): G. Bridel & C$^{ie}$.

Golay-Nicole A (1994) *La Vallée au jour le jour (1840-1900)*. Les Charbonnières (Switzerland): Editions Le Pélerin.

Hajdas I (2014) Radiocarbon: Calibration to Absolute Time Scale. in: Holland H, Turekian K (eds), *Treatise on Geochemistry (Second Edition) - Volume 14: Archaeology and Anthropology*. Oxford: Elsevier, pp. 37-43.

Hajdas I, Cristi C, Bonani G, Maurer M (2014) Textiles and radiocarbon dating. *Radiocarbon* 56: 637-643.

Hooke R LeB (2000) On the history of humans as geomorphic agents. *Geology* 28: 843-846.

Hope BK (2006) An examination of ecological risk assessment and management practices. *Environment International* 32: 983–995.

Lal R (1997) Degradation and resilience of soils. *Philosophical Transactions of the Royal Society B* 352: 997-1010.

Lavrieux M, Disnar JR, Chapron E, Bréheret JG, Jacob J, Miras Y, Reyss JL, Andrieu-Ponel V, Arnaud F (2013) 6700 yr sedimentary record of climatic and anthropogenic signals in Lake Aydat (French Massif Central). *The Holocene* 23: 1317-1328.

Layné JP (1671) *Vallée de Joux*. Map, Achives Communales de Morges.

Magny M, Peyron O, Gauthier E, Vannière B, Millet L, Vermot-Desroches B (2011) Quantitative estimates of temperature and precipitation changes over the last millennium from pollen and lake-level data at Lake Joux, Swiss Jura Mountains. *Quaternary Research* 75: 45-54.

Magny M, Gauthier E, Vannière B, Peyron O (2008) Paleohydrological changes and human-impact history over the last millenium recorded at Lake Joux in the Jura Mountains, Switzerland. *The Holocene* 18: 255-265.

Messerli B, Grosjean M, Hofer T, Nunez L, Pfister C (2000) From nature-dominated to human-dominated environmental changes. *Quaternary Science Reviews* 19: 459-479.

Meyers PA, Lallier-Vergès E (1999) Lacustrine sedimentary organic matter records of LateQuaternary paleoclimates. *Journal of Paleolimnology* 21: 345-372.

Mitchell EAD, van der Knaap WO, van Leeuwen JFN, Buttler A, Warner BG, Gobat JM (2001) The palaeoecological history of the Praz-Rodet bog (Swiss Jura) based on pollen, plant macrofossils and testate amoebae (Protozoa). *The Holocene* 11: 65-80.

Nicole JD (1840) *Recueil historique sur l'origine de la vallée du Lac-de-Joux, l'établissement de ses premiers habitants, celui des trois communautés dont elle est composée, et particulièrement du Chenit*. Lausanne (Switzerland): M. Ducloux.

Paquet G (2002) *Biologie et écologie de l'ombre commun (Thymallus thymallus L.) dans l'Orbe à la Vallée de Joux, canton de Vaud, Suisse*. PhD Thesis, University of Lausanne, Switzerland.

Piguet M (1895) *Histoire de l'horlogerie à la Vallée de Joux*. Le Sentier (Switzerland): J. Dupuis.

Piguet A (1946) *Le territoire et la commune du Lieu jusqu'en 1536*. Le Sentier (Switzerland): R. Dupuis.

Piguet A (1947) *La commune du Chenit, Tome 1. Le territoire du Chenit et la naissance de cette commune*. Le Sentier (Switzerland): R. Dupuis.

Piguet A (1952) *La commune du Chenit, Tome 2*. La commune du Chenit de 1646 à 1701. Le Sentier (Switzerland): R. Dupuis.

Piguet A (1971) *La commune du Chenit, Tome 3*. La commune du Chenit au XVIIIe siècle. Le Sentier (Switzerland): R. Dupuis.

Piguet A (1999) *La commune du Lieu de 1536 à 1646*. Les Charbonnières (Switzerland): Editions Le Pélerin.

Poynter JG, Eglinton G (1990) Molecular composition of three sediments from hole 717C: the Bengal Fan. In: Cochran JR, Stow DAV et al. (eds) *Proceedings of the Ocean Drilling Program, Scientific Results* 116, pp. 155-161.

Reinhard M, Gächter R, Wehrli B, Müller B (2005) Phosphorus retention in small constructed wetlands treating agricultural drainage water. *Journal of Environmental Quality* 34, 1251-1259.

Revel-Rolland M, Arnaud F, Chapron E, Desmet M, Givelet N, Alibert C, McCulloch M (2005) Sr and Nd isotopes as tracers of clastic sources in Lake le Bourget sediment (NW Alps, France) during the Little Ice Age: palaeohydrology implications. *Chemical Geology* 224: 183–200.

Rochat R (1995) *Supplément n°4 à l'histoire de la communauté du Lieu*. Les Charbonnières (Switzerland): Editions Le Pèlerin.

Rochat R (2006) *Une promenade historique autour du Lac Brenet*. Les Charbonnières (Switzerland): Editions Le Pèlerin.

Rumpel C, Chabbi A, Nunan N, Dignac MF (2009) Impact of land use change on the molecular composition of soil organic matter. *Journal of Analytical and Applied Pyrolysis* 85: 431–434.

Sala OE, Chapin FS, Armesto JJ, Berlow R, Bloomfield J, Dirzo R, Huber-Sanwald E, Huenneke LF, Jackson RB, Kinzig A, Leemans R, Lodge D, Mooney HA, Oesterheld M, Poff NL, Sykes MT,

Walker BH, Walker M, Wall DH (2000) Global biodiversity scenarios for the year 2100. *Science* 287: 1770-1774.

Shotyk W, Cheburkin AK, Appleby PG, Fankhauser A, Kramers JD (1996) Two thousand years of atmospheric arsenic, antimony, and lead deposition recorded in an ombrotrophic peat bog profile, Jura Mountains, Switzerland. *Earth and Planetary Science Letters* 145: E1-E7.

Shotyk W, Weiss D, Heisterkamp M, Cheburkin AK, Appleby PG, Adams FC (2002) New peat bog record of atmospheric lead pollution in Switzerland: Pb concentrations, enrichment factors, isotopic composition, and organolead species. *Environmental Science and Technology*: 36, 3893-3900.

Smith VH (2003) Eutrophication of freshwater and coastal marine ecosystems – a global problem. *Environmental Science and Pollution Research* 10: 126-139.

Snowball I, Hounslow MW, Nilsson A (2000) Geomagnetic and mineral magnetic characterization of the Anthropocene. in: Foster IDL (ed), *Tracers in Geomorphology*. Chichester: Wiley, pp. 119-142.

Swiss Federal Nuclear Safety Inspectorate (2016) Série Tchernobyl : le panache radioactif passe sur la Suisse. Available at: www.ensi.ch/de/2016/02/18/artikelserie-tschernobyl-die-radioaktive-wolke-zieht-ueber-die-schweiz (accessed 11.10.2016).

Synal HA, Stocker M, Suter M (2007) MICADAS: A new compact radiocarbon AMS system. *Nuclear Instruments and Methods in Physics Research Section B: Beam Interactions with Materials and Atoms* 259: 7-13.

Thevenon F, Poté J (2012) Water pollution history of Switzerland recorded by sediments of the large and deep perialpine lakes Lucerne and Geneva. *Water, Air and Soil Pollution* 223: 6157-6169.

Thevenon F, Guédron S, Chiaradia M, Loizeau JL, Poté J (2011) (Pre-) historic changes in natural and anthropogenic heavy metals deposition inferred from two contrasting Swiss Alpine lakes. *Quaternary Science Reviews* 30: 224-233.

Trouet V, Esper J, Graham NE, Baker A, Scourse JD, Frank DC (2009) Persistent positive North Atlantic Oscillation mode dominated the Medieval Climate Anomaly. *Science* 324: 78–80.

Vallotton JO (1708) *Vallée de Joux*. Map, Yale University (USA).

Vitousek PM, Mooney HA, Lubchenco J, Melillo JM (1997) Human domination of Earth's ecosystems. *Science* 277: 494-499.

Wacker L, Němec M, Bourquin J (2010) A revolutionary graphitisation system: fully automated, compact and simple. *Nuclear Instruments and Methods in Physics Research B* 268: 931-934.

Wegmüller S (1966) Über die spät- und postglaziale Vegetationsgeschichte des südwestlichen Jura. *Beiträge zur geobotanischen landesaufnahme der Schweiz* 48: 1-142.

Whittle D (2006) Paléoécologie et géochimie isotopique des ostracodes du lac de Joux (Jura, Suisse). Master Thesis, University of Geneva (Switzerland).

Wilcock DN (1999) River and inland water environments. In: Nath B, Hens L, Compton P, Devuyst D (eds) *Environmental management in practice, volume 3*, pp. 328.

Wilkinson BH (2005) Humans as geologic agents: A deeptime perspective. *Geology* 33: 161-164.

Wirth SB, Gilli A, Niemann H, Dahl TW, Ravasi D, Sax N, Hamann Y, Peduzzi R, Peduzzi S, Tonolla M, Lehmann MF, Anselmetti FS (2013) Combining sedimentological, trace metal (Mn, Mo) and molecular evidence for reconstructing past water-column redox conditions: The example of meromictic Lake Cadagno (Swiss Alps). *Geochimica et Cosmochimica Acta* 120: 220–238.

Zhang Y, Liu X, Lin Q, Gao G, Wang J, Wang G (2014) Vegetation and climate change over the past 800 years in the monsoon margin of northeastern China reconstructed from *n*-alkanes from the Great Hinggan Mountain ombrotrophic peat bog. *Organic Geochemistry* 76: 128-135.

**Figures captions**

**Figure 1.** Geographical setting of Lake Joux catchment and location of coring site. Also shown are the locations of karstic caves (according to Aubert, 1943) and former iron mines (according to Piguet, 1895; Rochat, 2006). Inset: location of Lake Joux. L: Liechtenstein; a.s.l.: above sea level.

**Figure 2.** Description, lithology and correlation of the two cores, sedimentological units and depth-age model constructed from $^{14}C_{macrofossils}$, $^{137}Cs$ and $^{210}Pb$ measurements.

**Figure 3.** Results of PCA, showing Principal Components 1 versus 2. Left: elements considered for the PCA (loadings). Right: corresponding map of the distribution of stratigraphic units 1 - 5 (scores).

**Figure 4.** Comparison of XRF counts and ICP-MS measurements. Black dots and values: all depths, except the lowest 14 cm of the core. Grey dots: values of the lowest 14 cm of the core. Grey values: $R^2$ for the whole set of values (including the lowest 14 cm). Black values: $R^2$, excluding the lowest 14 cm of the core. Lines: linear regressions.

**Figure 5.** Organic and inorganic data ($CaCO_3$, $C_{org}$, phosphorus, $\delta^{13}C$, magnetic susceptibility, XRF, *n*-alkane ratios, sedimentation rate, Ti flux, K/Ti, grain size) obtained from cores JOU-13-02 and JOU-14-01. ACL: Average Chain Length; CPI: Carbon Preference Index. Grey bars show the location of the dark layers.

**Figure 6.** Summary of the human-impact history and of the inputs (autochthonous and detrital) and erosion (physical and chemical) patterns, as interpreted from the available data. Core lithology symbols: refer to Figure 2.

**Table captions**

**Table 1.** AMS radiocarbon dates obtained from JOU-13-02 core.

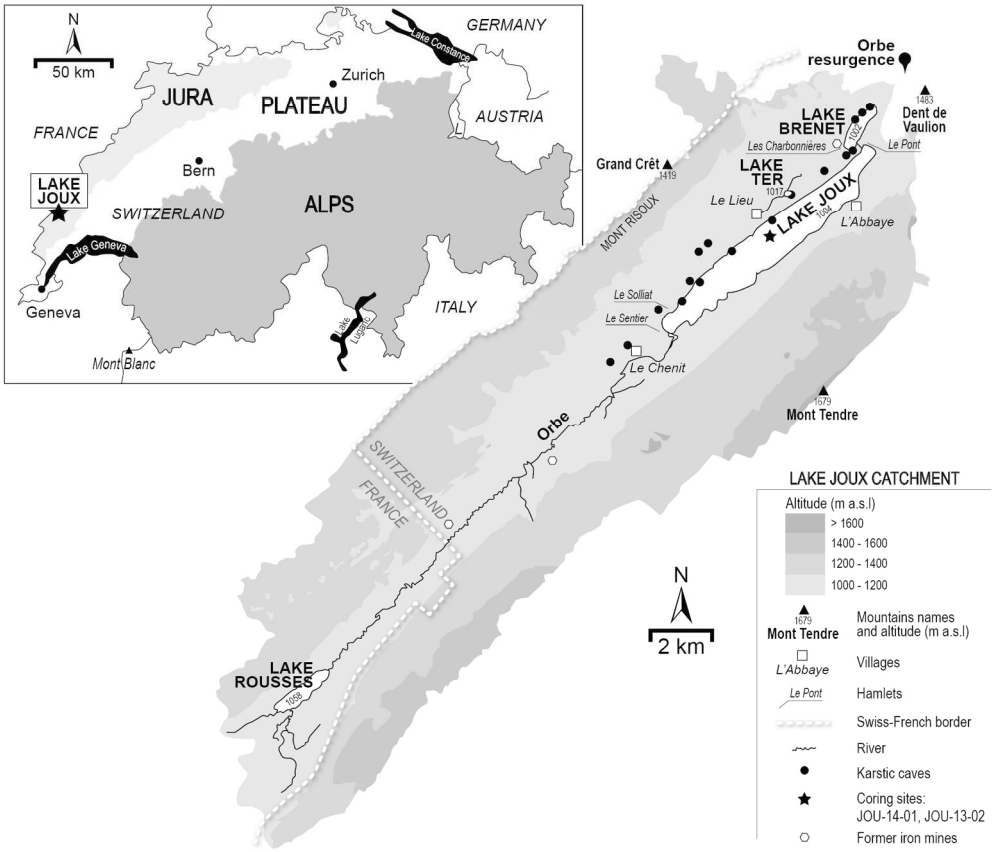


Figure 1. Geographical settings of Lake Joux catchment and coring site location. Location of karstic caves according to Aubert (1943), of former iron mines according to Piguet (1895) and Rochat (2006). Inset: location of Lake Joux. L: Liechtenstein; a.s.l.: above sea level.

326x279mm (150 x 150 DPI)

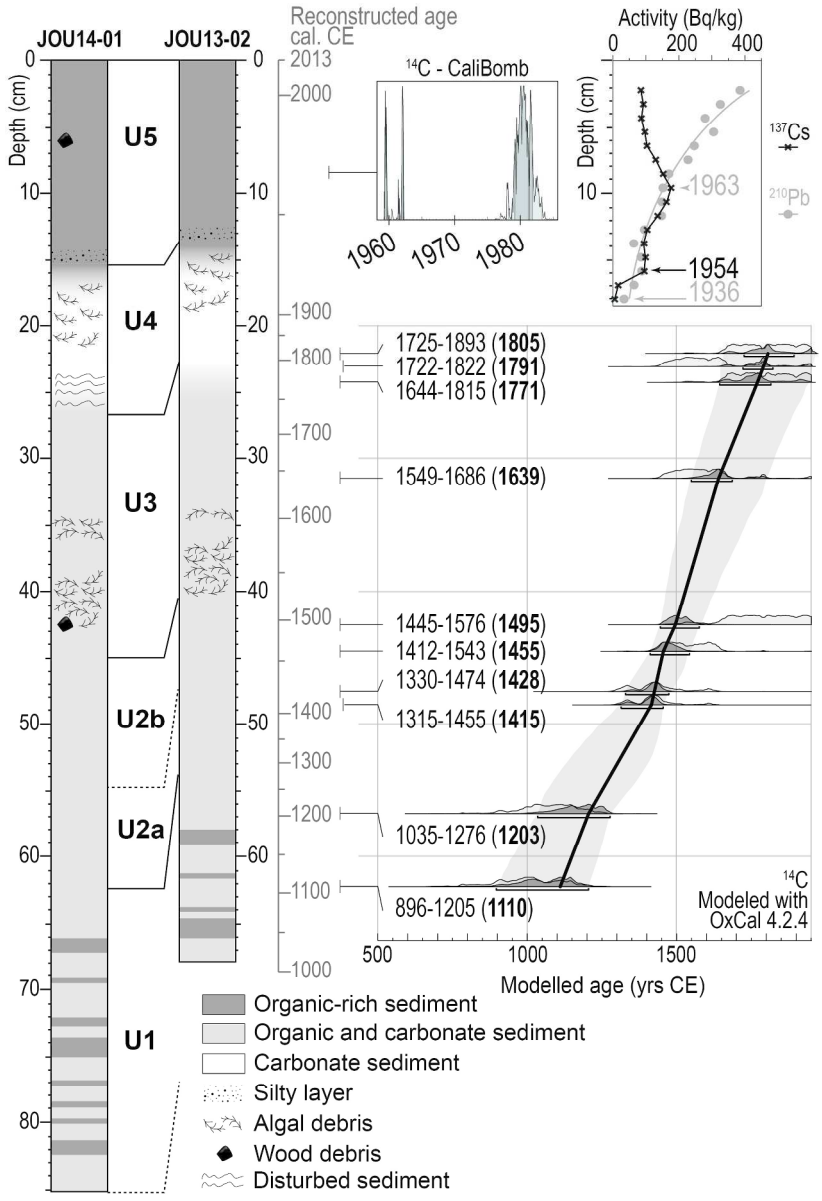


Description, lithology and correlation of the two cores, sedimentological units and depth-age model constructed from $^{14}C_{macrofossils}$, $^{137}Cs$ and $^{210}Pb$ measurements.

Fig. 2

200x296mm (300 x 300 DPI)

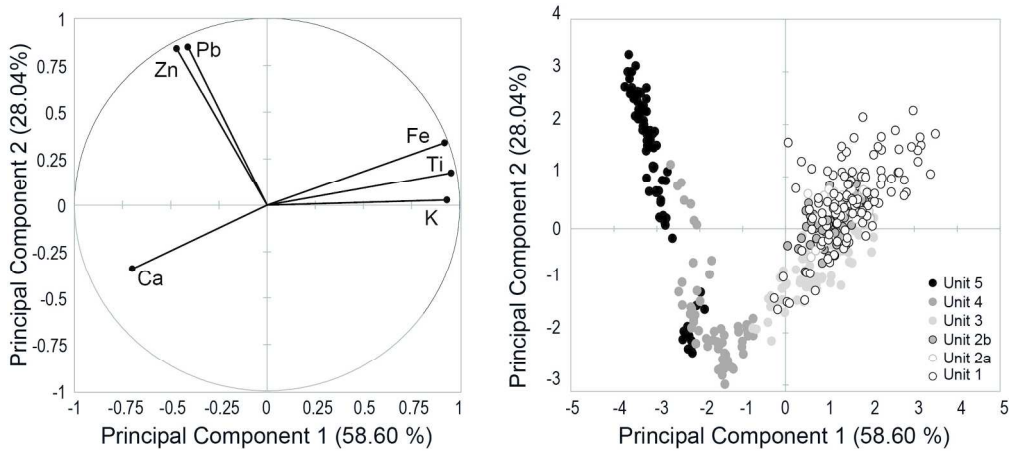


Results of the PCA according to dimensions 1 and 2. Left: elements considered for the PCA. Right: map of the units distribution.

Fig. 3

188x84mm (300 x 300 DPI)

eer Review

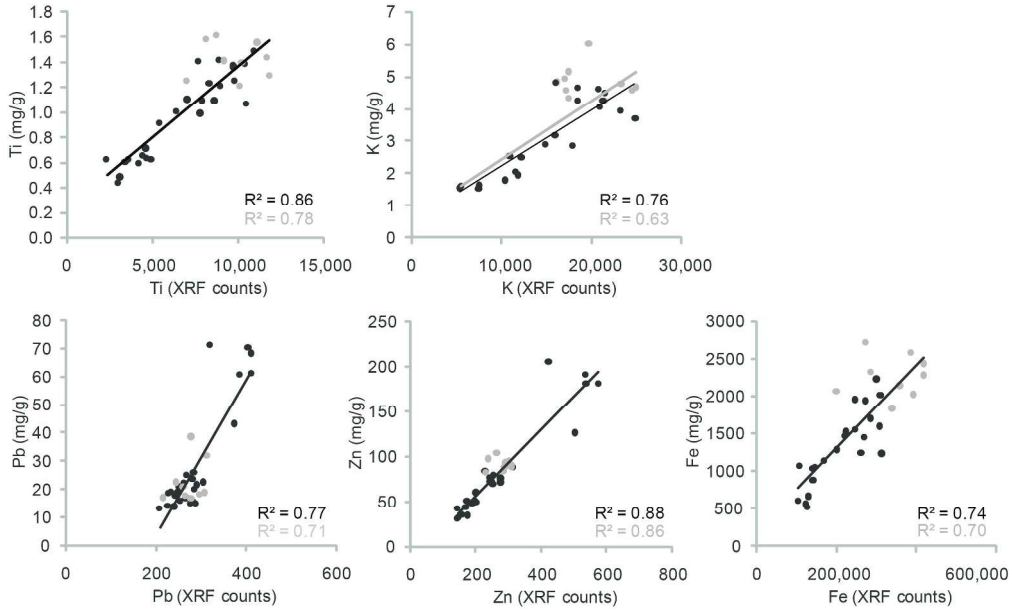


Comparison of XRF counts and ICP-MS measurements. Black dots and values: all depths, except the lowest 14 cm of the core. Grey dots: values of the lowest 14 cm of the core. Grey values: $R^2$ for the whole set of values (including the lowest 14 cm). Black values: $R^2$, excluding the lowest 14 cm of the core. Lines: linear regressions.

Fig. 4

273x165mm (300 x 300 DPI)

Review

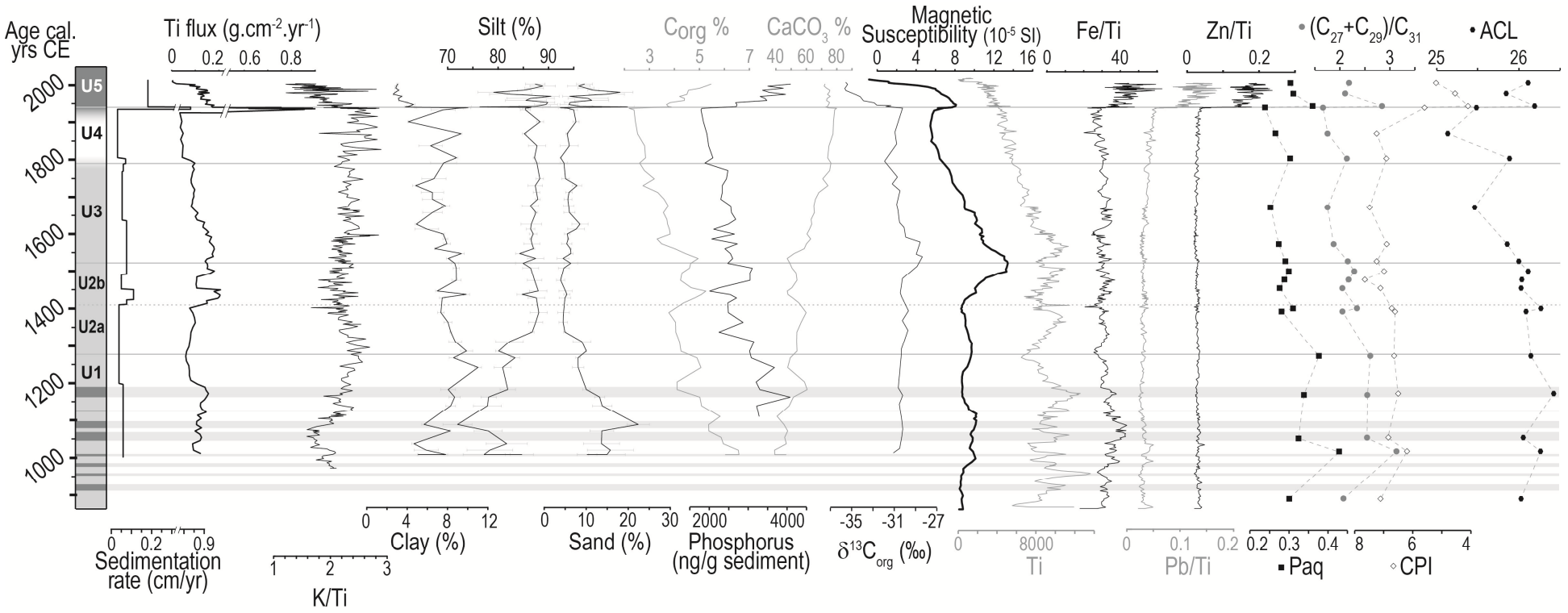
Age cal. yrs CE
Ti flux (g.cm-2.yr-1)
Silt (%)
Corg %
CaCO3 %
Magnetic Susceptibility (10-5 SI)
Fe/Ti
Zn/Ti
(C27+C29)/C31
ACL
U5
U4
U3
U2b
U2a
U1
Sedimentation rate (cm/yr)
K/Ti
Clay (%)
Sand (%)
Phosphorus (ng/g sediment)
δ13Corg (‰)
Ti
Pb/Ti
Paq
CPI

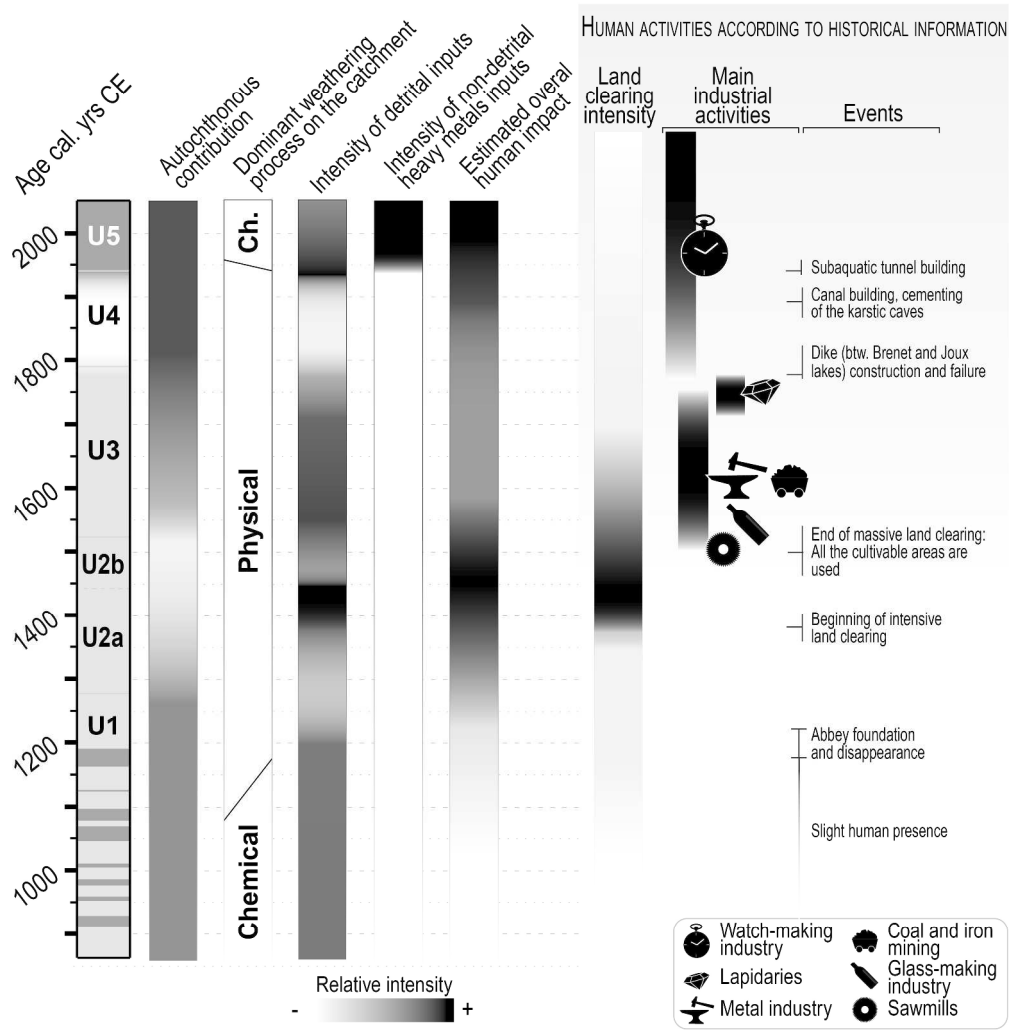


Summary of the human-impact history and of the inputs (autochthonous and detrital) and erosion (physical and chemical) patterns, as interpreted from the available data. Core lithology symbols: refer to Figure 2.
Fig. 6
323x336mm (300 x 300 DPI)

| Core | Depth (cm) | AMS $^{14}$C age (yr BP) | $\delta^{13}$C | Calibrated age (2σ range) | | Laboratory number | Material |
|---|---|---|---|---|---|---|---|
| | | | | cal. yr BP | cal. yr CE | | |
| JOU 13-02 | 9.6-10.6 | -2000 ± 120 | -40.8 | **-27 - -35 (-31)** | **1977 - 1985 (1981)** | ETH-58081 | Leaf |
| | *16.6-17.6* | *>45000* | *-38.1* | - | - | *ETH-58083* | *Wood* |
| | 21.6-22.6 | 135 ± 75 | -32.9 | 291 – 243<br>**225 – 57 (145)**<br>31 – -18 | 1659 – 1707<br>**1725 – 1893 (1805)**<br>1919 – 1968 | ETH-58084 | Wood |
| | 22.6-23.6 | 300 ± 75 | -21.3 | 302 – 252<br>**228 – 128 (159)**<br>98 – 70<br>41 – -4 | 1648 – 1698<br>**1722 – 1822 (1791)**<br>1852 – 1880<br>1909 – 1954 | ETH-58085 | Wood |
| | 23.6-25 | 150 ± 70 | -23.1 | **306 – 135 (179)**<br>117 – 84<br>78 – 72<br>67 – 6 | **1644 – 1815 (1771)**<br>1833 – 1866<br>1872 – 1878<br>1883 – 1944 | ETH-58086 | Wood and insect parts |
| | 31-32 | 310 ± 70 | -27.6 | **401 – 264 (311)**<br>218 – 150 | **1549 – 1686 (1639)**<br>1732 – 1800 | ETH-58087 | Wood |
| | 42-43 | 145 ± 100 | -41 | **505 – 374 (455)** | **1445 – 1576 (1495)** | ETH-58088 | Insect parts |
| | 44-45 | 385 ± 75 | -31.6 | **538 – 407 (495)** | **1412 – 1543 (1455)** | ETH-58089 | Leaf |
| | 47-48 | 495 ± 85 | -42.3 | **620 – 476 (522)** | **1330 – 1474 (1428)** | ETH-58090 | Conifer needle and terrestrial vegetal debris |
| | 48-49 | 495 ± 70 | -35.4 | **635 – 495 (535)** | **1315 – 1455 (1415)** | ETH-58091 | Terrestrial vegetal debris |
| | 56-57.4 | 970 ± 90 | -40.1 | **915 – 674 (747)** | **1035 – 1276 (1203)** | ETH-58092 | Terrestrial vegetal debris, insect parts and pollen |
| | 61.4-63 | 1030 ± 90 | -52.3 | **1054 – 745 (840)** | **896 – 1205 (1110)** | ETH-58094 | Leaf |
| | *69-70* | *-475 ± 75* | *-51.8* | - | - | *ETH-58095* | *Leaf* |

For Peer Review